Density Functional Theory Model of Adsorption on Amorphous and Microporous Silica Materials

Peter I. Ravikovitch* and Alexander V. Neimark[†,‡]

Center for Modeling and Characterization of Nanoporous Materials, TRI/Princeton, 601 Prospect Avenue, Princeton, New Jersey 08540

We present a novel quenched solid density functional theory (QSDFT) model of adsorption on heterogeneous surfaces and porous solids, which accounts for the effects of surface roughness and microporosity. Within QSDFT, solid atoms are considered as quenched component(s) of the solid−fluid system with given density distribution(s). Solid−fluid intermolecular interactions are split into hard-sphere repulsive and mean-field attractive parts. The former are treated with the multicomponent fundamental measure density functional. Capabilities of QSDFT are demonstrated by drawing on the example of adsorption on amorphous silica materials. We show that, using established intermolecular potentials and a realistic model for silica surfaces, QSDFT quantitatively describes adsorption/desorption isotherms of Ar and Kr on reference MCM-41, SBA-15, and LiChrosphere materials in a wide range of relative pressures. QSDFT offers a systematic approach to the practical problems of characterization of microporous, mesoporous, and amorphous silica materials, including an assessment of microporosity, surface roughness, and adsorption deformation. Predictions for the pore diameter and the extent of pore surface roughness in MCM-41 and SBA-15 materials are in very good agreement with recent X-ray diffraction studies.

1. Introduction

Density functional theory (DFT) (see refs 1 and 2 for reviews) has found great utility in modeling adsorbed phases[3−7] and developing calculation methods for pore size characterization from experimental adsorption isotherms.[8−11] In our earlier publications, it has been demonstrated that nonlocal density functional theory (NLDFT)[12,13] with suitably chosen parameters for fluid−fluid and fluid−solid interactions[14] quantitatively predicts the positions of capillary condensation and desorption transitions of simple fluids (Ar, N_2) in ordered nanoporous materials with cylindrical[6,15] and spherical[16] pores, such as MCM-41, SBA-15, and SBA-16. A set of NLDFT-based methods for calculating pore size distributions (PSD) in materials of different origin has been developed. Their validity has been verified by

extensive comparisons with independent estimates of pore sizes in reference samples[7] and small-angle X-ray and neutron scattering (SAXS/SANS) methods.[17]

However, the NLDFT models imply that the pore walls are smooth and homogeneous, and thus, they do not account for the energetic and/or geometrical heterogeneity inherent to real silica surfaces. Typically, NLDFT models operate with fluids confined to pores of simple geometries (slit, cylinder, sphere). The models are effectively one-dimensional, since the solid−fluid potential and the fluid density vary only in the direction normal to the pore wall. The consequence of this simplification is that it induces a strong layering in the adsorbed phase, especially at low temperatures. Therefore, adsorption isotherms exhibit artificial steps in the region of multilayer adsorption.[6] This deficiency of one-dimensional NLDFT models is well-documented.[18,19] The layering transition steps on the theoretical isotherms cause artificial gaps on the calculated pore size distributions.[18,19] For example, for N_2 on graphite at 77 K, the monolayer transition in NLDFT occurs at the same pressure as the pore filling in ∼1 nm wide slit pore, which results in a prominent false gap on the calculated pore size distribution histograms.[19]

Another crucial problem is a proper account for the surface roughness and microporosity, which are inherent to a large number of novel polymer-templated silica and organosilica materials, such as, for example, SBA-15.[15,20−23] By the standard comparison or *t*-plot methods,[24] the volume of micropores cannot be reliably

* Corresponding author: e-mail ravikovi@triprinceton.org.
† Present address: Department of Chemical and Biochemical Engineering, Rutgers, The State University of New Jersey, 98 Brett Rd., Piscataway, NJ 08854-8058.
‡ E-mail: aneimark@rci.rutgers.edu.

(1) Evans, R. In *Fundamentals of Inhomogeneous Fluids*; Henderson, D., Ed.; Marcel Dekker: New York, 1992; Chapter 5.
(2) Wu, J. Z. *AIChE J.* **2006**, *52*, 1169−1193.
(3) Evans, R.; Marconi, U. M. B.; Tarazona, P. *J. Chem. Soc., Faraday Trans. 2* **1986**, *82*, 1763−1787.
(4) Peterson, B. K.; Heffelfinger, G. S.; Gubbins, K. E.; van Swol, F. *J. Chem. Phys.* **1990**, *93*, 679−685.
(5) Balbuena, P. B.; Gubbins, K. E. *Langmuir* **1993**, *9*, 1801−1814.
(6) Ravikovitch, P. I.; O'Domhnaill, S. C.; Neimark, A. V.; Schuth, F.; Unger, K. K. *Langmuir* **1995**, *11*, 4765−4772.
(7) Neimark, A. V.; Ravikovitch, P. I.; Vishnyakov, A. *J. Phys.: Condens. Matter* **2003**, *15*, 347−365.
(8) Seaton, N. A.; Walton, J.; Quirke, N. *Carbon* **1989**, *27*, 853−861.
(9) Lastoskie, C.; Gubbins, K. E.; Quirke, N. *J. Phys. Chem.* **1993**, *97*, 4786−4796.
(10) Olivier, J. P. *J. Porous Mater.* **1995**, *2*, 217.
(11) Ravikovitch, P. I.; Wei, D.; Chueh, W. T.; Haller, G. L.; Neimark, A. V. *J. Phys. Chem. B* **1997**, *101*, 3671−3679.
(12) Tarazona, P. *Phys. Rev. A* **1985**, *31*, 2672−2679.
(13) Tarazona, P.; Marconi, U. M. B.; Evans, R. *Mol. Phys.* **1987**, *60*, 573−595.
(14) Ravikovitch, P. I.; Vishnyakov, A.; Neimark, A. V. *Phys. Rev. E* **2001**, *64*, 011602.
(15) Ravikovitch, P. I.; Neimark, A. V. *J. Phys. Chem. B* **2001**, *105*, 6817−6823.
(16) Ravikovitch, P. I.; Neimark, A. V. *Langmuir* **2002**, *18*, 1550−1560.

(17) Thommes, M.; Smarsly, B.; Groenewolt, M.; Ravikovitch, P. I.; Neimark, A. V. *Langmuir* **2006**, *22*, 756−764.
(18) Olivier, J. P. *Carbon* **1998**, *36*, 1469−1472.
(19) Ravikovitch, P. I.; Vishnyakov, A.; Russo, R.; Neimark, A. V. *Langmuir* **2000**, *16*, 2311−2320.
(20) Imperor-Clerc, M.; Davidson, P.; Davidson, A. *J. Am. Chem. Soc.* **2000**, *122*, 11925−11933.
(21) Kruk, M.; Jaroniec, M.; Ko, C. H.; Ryoo, R. *Chem. Mater.* **2000**, *12*, 1961−1968.
(22) Galarneau, A.; Cambon, H.; Di Renzo, F.; Fajula, F. *Langmuir* **2001**, *17*, 8328−8335.
(23) Fenelonov, V. B.; Derevyankin, A. Y.; Kirik, S. D.; Solovyov, L. A.; Shmakov, A. N.; Bonardet, J. L.; Gedeon, A.; Romannikov, V. N. *Microporous Mesoporous Mater.* **2001**, *44*, 33−40.

estimated due to a competition between micropore filling and multilayer adsorption on a rough surface of low-density "corona".

A straightforward approach to account for surface heterogeneity is to invoke the concept of adsorption energy distribution[25] and to present the experimental isotherm as a combination of isotherms on surface patches with different energies of adsorption.[10] Another approach is to use a heterogeneous solid−fluid interaction potential. Maddox et al.[26] performed MC simulations of adsorption in cylindrical pores of MCM-41 with a radially and axially dependent potential and obtained good agreement with the experimental data. Recently, toluene adsorption on MCM-41 has been successfully simulated by use of a model with randomly distributed attractive and repulsive sites on the pore walls.[27]

Atomic-level heterogeneity can be introduced by considering in the simulations/models the structure of real silica surfaces.[28−34] Bakaev and Steele[35] reported grand canonical ensemble Monte Carlo (GCEMC) simulations of Ar adsorption on amorphous oxides modeled as a dense random packing of oxygen ions (Bernal surface). They demonstrated that the geometrical corrugation of the surface leads to smooth multilayer isotherms of type II typically observed on various oxides.[24] In the submonolayer region, the isotherms are sensitive to the detail of the interatomic interaction parameters and distribution of adsorption centers.[35,36] Effects of surface corrugation and roughness have been considered in molecular models of silica glasses and amorphous silicas[37−39] and MCM-41.[40−46]

Unfortunately, in the framework of conventional NLDFT models, any detailed description of chemical and/or geometrical heterogeneities requires computationally expensive two- or three-dimensional NLDFT formulations.[47−50] In this case, the main advantage of one-dimensional NLDFT models for PSD calculations, namely, their computational efficiency, is lost. In the conventional NLDFT framework, the fluid−fluid interactions are split into hard-sphere (HS) repulsive interactions and mean-field attractive interactions. Recently, Ustinov et al.[50−52] developed a modification of one-component Tarazona's NLDFT[12,13] that is capable of generating smooth isotherms in the region of mono- and polymolecular adsorption. The authors used the Weeks−Chandler−Andersen (WCA) scheme[53] for solid−fluid attractive interactions and reduced the contribution from the HS repulsive interactions in the vicinity of the solid surface, which decreased the layered structure of the fluid. The parameters of the model were fitted to obtain good agreement with experimental N_2 and Ar adsorption data on MCM-41,[52] nonporous amorphous silica,[51] and carbon.[54]

In this paper we present a novel approach to accounting for surface roughness and heterogeneity within one-dimensional NLDFT, which was briefly outlined in ref 55. In contrast to the existing approaches, in which the pore wall roughness was effectively accounted for within one-component DFT models by modifying the repulsive HS term in the proximity of the solid,[50] we consider a multicomponent DFT in which the solid atoms are represented as quenched component(s) of the solid−fluid system, with given density distribution(s), rather than the source of an external potential. The fluid is an "annealed" component. Quenched-annealed systems as models of disordered porous media have been studied by liquid integral equation theories.[56−59] Schmidt[60−62] developed a quenched-annealed DFT for the systems with hard-core and ideal interactions. Quenched-annealed DFT is a powerful method in which the solid component of the solid−fluid mixture is described on the level of one-body density distribution that can be strongly inhomogeneous.[62] Our model, named the quenched solid density functional theory (QSDFT), is an extension of the quenched-annealed DFT of Schmidt[60,61] to solid−fluid Lennard-Jones systems with attractive interactions. Recently, a simplified "quenched-annealed" model of the fluid−solid interface was described for a particular case of adsorption of argon on solid argon,[50] where no distinction was made between fluid and solid particles, and their contribution to the free energy of HS interactions was described within the one-dimensional Tarazona's NLDFT.

In QSDFT, we consider that solid−fluid and fluid−fluid interactions are split into hard-sphere repulsive and mean-field attractive parts. Hard-sphere interactions are treated with the multicomponent fundamental measure theory (FMT) functional[63,64] for quenched-annealed systems.[60] Attractive interactions are treated with the WCA attractive potential,[53] similarly to ref 50. We demonstrate that the solid density distribution, introduced in QSDFT to account for the surface roughness, eliminates strong layering of the fluid near the walls. Moreover, the effects of pore wall microporosity can be naturally incorporated into the model by using a reduced density of solid. We present examples of calculated adsorption isotherms, which are in quantitative

(24) Gregg, S. J.; Sing, K. S. W. *Adsorption, Surface Area and Porosity*; Academic Press: New York, 1982.

(25) Jaroniec, M.; Madey, R. *Physical Adsorption on Heterogeneous Solids*; Elsevier: Amsterdam, 1988.

(26) Maddox, M. W.; Olivier, J. P.; Gubbins, K. E. *Langmuir* **1997**, *13*, 1737−1745.

(27) Ravikovitch, P. I.; Vishnyakov, A.; Neimark, A. V.; Carrott, M.; Russo, P. A.; Carrott, P. J. *Langmuir* **2006**, *22*, 513−516.

(28) (a) Garofalini, S. H. *J. Chem. Phys.* **1983**, *78*, 2069−2072. (b) Feuston, B. P.; Garofalini, S. H. *J. Chem. Phys.* **1988**, *89*, 5818−5824.

(29) MacElroy, J. M. D.; Raghavan, K. *J. Chem. Phys.* **1990**, *93*, 2068−2079.

(30) Brodka, A.; Zerda, T. W. *J. Chem. Phys.* **1991**, *95*, 3710−3718.

(31) Kohler, A. E.; Garofalini, S. H. *Langmuir* **1994**, *10*, 4664−4669.

(32) Stallons, J. M.; Iglesia, E. *Chem. Eng. Sci.* **2001**, *56*, 4205−4216.

(33) Roder, A.; Kob, W.; Binder, K. *J. Chem. Phys.* **2001**, *114*, 7602−7614.

(34) Rarivomanantsoa, M.; Jund, P.; Jullien, R. *J. Phys.: Condens. Matter* **2001**, *13*, 6707−6718.

(35) (a) Bakaev, V. A.; Steele, W. A. *Langmuir* **1992**, *8*, 148−154. (b) Bakaev, V. A.; Steele, W. A. *Langmuir* **1992**, *8*, 1379−1384.

(36) Bakaev, V. A.; Steele, W. A.; Bakaeva, T. I.; Pantano, C. G. *J. Chem. Phys.* **1999**, *111*, 9813−9821.

(37) Gelb, L. D.; Gubbins, K. E. *Langmuir* **1998**, *14*, 2097−2111.

(38) de Torre, L. E. C.; Flores, E. S.; Bottani, E. J. *Langmuir* **2000**, *16*, 1896−1901.

(39) Coasne, B.; Pellenq, R. J. M. *J. Chem. Phys.* **2004**, *120*, 2913−2922.

(40) Feuston, B. P.; Higgins, J. B. *J. Phys. Chem.* **1994**, *98*, 4459−4462.

(41) He, Y. F.; Seaton, N. A. *Langmuir* **2003**, *19*, 10132−10138.

(42) Kuchta, B.; Llewellyn, P.; Denoyel, R.; Firlej, L. *Colloids Surf. A:Physicochem. Eng. Aspects* **2004**, *241*, 137−142.

(43) Carvalho, A. J. P.; Ferreira, T.; Candeias, A. J. E.; Ramalho, J. P. P. *THEOCHEM: J. Mol. Struct.* **2005**, *729*, 65−69.

(44) Sonwane, C. G.; Jones, C. W.; Ludovice, P. J. *J. Phys. Chem. B* **2005**, *109*, 23395−23404.

(45) Fox, J. P.; Bates, S. P. *Langmuir* **2005**, *21*, 4746−4754.

(46) Coasne, B.; Hung, F. R.; Pellenq, R. J. M.; Siperstein, F. R.; Gubbins, K. E. *Langmuir* **2006**, *22*, 194−202.

(47) Henderson, D.; Sokolowski, S.; Wasan, D. *Phys. Rev. E* **1998**, *57*, 5539−5543.

(48) Frink, L. J. D.; Salinger, A. G. *J. Comput. Phys.* **2000**, *159*, 407−424.

(49) Frink, L. J. D.; Salinger, A. G. *J. Chem. Phys.* **2003**, *118*, 7466−7476.

(50) Ustinov, E. A.; Do, D. D. *Adsorption* **2005**, *11*, 455−477.

(51) Ustinov, E. A.; Do, D. D.; Jaroniec, M. *Appl. Surf. Sci.* **2005**, *252*, 548−561.

(52) Ustinov, E. A.; Do, D. D.; Jaroniec, M. *Appl. Surf. Sci.* **2005**, *252*, 1013−1028.

(53) Weeks, J. D.; Chandler, D.; Andersen, H. C. *J. Chem. Phys.* **1971**, *54*, 5237.

(54) Ustinov, E. A.; Do, D. D.; Fenelonov, V. B. *Carbon* **2006**, *44*, 653−663.

(55) Ravikovitch, P. I.; Neimark, A. V. In *Characterisation of Porous Solids VII*; Llewellyn, P. L., Rouquerol, J., Rodrigues-Reinoso, F., Seaton, N. A., Eds.; Elsevier: Amsterdam, 2005; Vol. 160, pp 9−16.

(56) Madden, W. G.; Glandt, E. D. *J. Stat. Phys.* **1988**, *51*, 537−558.

(57) Given, J. A.; Stell, G. *J. Chem. Phys.* **1992**, *97*, 4573−4574.

(58) Dong, W.; Kierlik, E.; Rosinberg, M. L. *Phys. Rev. E* **1994**, *50*, 4750−4753.

(59) Pizio, O.; Sokolowski, S. *Phys. Rev. E* **1997**, *56*, R63−R66.

(60) Schmidt, M. *Phys. Rev. E* **2002**, *66*, 041108.

(61) Schmidt, M. *Phys. Rev. E* **2003**, *68*, 021106.

(62) Schmidt, M. *J. Phys.: Condens. Matter* **2005**, *17*, S3481−S3486.

(63) Rosenfeld, Y. *Phys. Rev. Lett.* **1989**, *63*, 980−983.

(64) Kierlik, E.; Rosinberg, M. L. *Phys. Rev. A* **1990**, *42*, 3382−3387.

agreement with experimental measurements of adsorption on MCM-41, nonporous amorphous silica, and polymer-templated SBA-15 silica materials with a minimal number of adjustable parameters.

The paper is organized as follows. In section 2 we review conventional NLDFT models and describe the QSDFT approach. Further, we consider limiting cases, such as hard spheres near a hard wall (section 3.1), adsorption in a hard-sphere matrix (section 3.2), and fluid in slit pores with attractive walls of various degree of smoothness (section 3.3). In section 3.4, we develop a QSDFT model for amorphous silicas and apply this model to Ar adsorption on MCM-41 (section 3.5) and nonporous Li-Chrosphere silica (section 3.6). In section 3.7, we study Kr adsorption on SBA-15 material based on the surface model obtained from X-ray diffraction studies of SBA-15. In section 3.8 we present example of calculations of solvation (disjoining) pressure isotherm in cylindrical pores of silica materials. Finally, we conclude that QSDFT provides a systematic framework for modeling adsorption on amorphous silica materials and characterizing surface roughness and microporosity, as well as for analyzing such fine effects as adsorption-induced deformation.

2. Theory

2.1. Conventional Nonlocal Density Functional Theory. In the conventional NLDFT description of a single component fluid in a pore,[1] the solid walls are considered as the source of an external potential $U_{ext}(\mathbf{r})$. The grand thermodynamic potential of the confined fluid, $\Omega[\rho(\mathbf{r})]$, is written as a functional of the one-body fluid density distribution, $\rho(\mathbf{r})$:

$$\Omega[\rho(\mathbf{r})] = F_{id}[\rho(\mathbf{r})] + F_{ex}[\rho(\mathbf{r})] +$$
$$\tfrac{1}{2}\int\int d\mathbf{r}\, d\mathbf{r}'\, \rho(\mathbf{r})\rho(\mathbf{r}')u_{ff}(|\mathbf{r} - \mathbf{r}'|) - \int d\mathbf{r}\, \rho(\mathbf{r})[\mu - U_{ext}(\mathbf{r})] \quad (1)$$

Here $F_{id}[\rho]$ and $F_{ex}[\rho]$ are the ideal and excess components of the Helmholtz free energy of the reference hard-sphere fluid, μ is the chemical potential, and $u_{ff}(|\mathbf{r} - \mathbf{r}'|)$ is the attractive part of the fluid−fluid intermolecular potential, treated in a mean-field fashion, for example, with the WCA scheme:[53]

$$u_{ff}(r) = \begin{cases} -\epsilon_{ff} & r < 2^{1/6}\sigma_{ff} \\ 4\epsilon_{ff}[(\sigma_{ff}/r)^{12} - (\sigma_{ff}/r)^6] & r \geq 2^{1/6}\sigma_{ff} \end{cases} \quad (2)$$

where ϵ_{ff} and σ_{ff} are the well depth and distance parameters of the Lennard-Jones (LJ) potential.

To determine the fluid density distribution, the functional is minimized with respect to $\rho(\mathbf{r})$ to obtain the Euler−Lagrange equation:

$$\rho(\mathbf{r}) = \Lambda^{-3}\exp\{c^{(1)}(\mathbf{r}; [\rho]) - \beta\int d\mathbf{r}'\, \rho(\mathbf{r})u_{ff}(|\mathbf{r} - \mathbf{r}'|) + \beta\mu - \beta U_{ext}(\mathbf{r})\} \quad (3)$$

where $c^{(1)}(\mathbf{r}; [\rho]) = -\beta\delta F_{ex}[\rho(\mathbf{r})]/\delta\rho(\mathbf{r})$ is the one-particle direct correlation function expressed as the functional derivative of the excess Helmholtz free energy of the HS fluid, Λ is the de Broglie wavelength, and $\beta = 1/k_B T$. The hard-sphere term $c^{(1)}(\mathbf{r}; [\rho])$ is usually taken either from Tarazona's SDA[12,13] or from Rosenfeld's FMT[63] functionals. Explicit expressions can be found elsewhere.[14,65−68]

2.2. Quenched Solid Density Functional Theory. QSDFT represents NLDFT in which solid and fluid are treated as a

multicomponent system. For simplicity, we consider a two-component case. The solid is considered as a "quenched" component with a given density distribution $\rho_S(\mathbf{r})$, and the fluid is considered as a "mobile" (or "annealed") component, whose density $\rho(\mathbf{r})$ is found from the functional minimization.

The grand potential functional of the fluid−solid system is given in the following general form:

$$\Omega_{sf}[\rho_S(\mathbf{r}); \rho(\mathbf{r})] = F_{id}[\rho(\mathbf{r})] + F_{id}[\rho_S(\mathbf{r})] + F_{ex}[\rho_S(\mathbf{r}); \rho(\mathbf{r})] +$$
$$\tfrac{1}{2}\int\int d\mathbf{r}\, d\mathbf{r}'\, \rho(\mathbf{r})\rho(\mathbf{r}')u_{ff}(|\mathbf{r} - \mathbf{r}'|) +$$
$$\tfrac{1}{2}\int\int d\mathbf{r}\, d\mathbf{r}'\, \rho_S(\mathbf{r})\rho_S(\mathbf{r}')u_{ss}(|\mathbf{r} - \mathbf{r}'|) +$$
$$\int\int d\mathbf{r}\, d\mathbf{r}'\, \rho(\mathbf{r})\rho_S(\mathbf{r}')u_{sf}(|\mathbf{r} - \mathbf{r}'|) - \mu\int d\mathbf{r}\, \rho(\mathbf{r}) - \mu_S\int d\mathbf{r}\, \rho_S(\mathbf{r})$$
$$(4)$$

In general, eq 4 is symmetric with respect to fluid and solid components. Similarly to the fluid−fluid intermolecular interactions, we treat solid−fluid interactions perturbatively and split the solid−fluid intermolecular potential into repulsive hard-sphere and attractive parts. That is, the solid is modeled as a compound of hard-core spheres, interacting with the fluid molecules via attractive potential $u_{sf}(r)$. The key term here is $F_{ex}[\rho_S(\mathbf{r}); \rho(\mathbf{r})]$, the excess free energy of the solid−fluid HS mixture, in which solid is a quenched component. However, since minimization is not performed with respect to solid density $\rho_S(\mathbf{r})$, we can omit terms related to ideal gas contribution to the solid free energy $F_{id}[\rho_S(\mathbf{r})]$, solid−solid interactions $u_{ss}(r)$, and solid chemical potential μ_S. As a result, we can write the grant potential functional for the fluid component as:

$$\Omega[\rho_S(\mathbf{r}); \rho(\mathbf{r})] = F_{id}[\rho(\mathbf{r})] + \tilde{F}_{ex}[\rho_S(\mathbf{r}); \rho(\mathbf{r})] +$$
$$\tfrac{1}{2}\int\int d\mathbf{r}\, d\mathbf{r}'\, \rho(\mathbf{r})\rho(\mathbf{r}')u_{ff}(|\mathbf{r} - \mathbf{r}'|) +$$
$$\int\int d\mathbf{r}\, d\mathbf{r}'\, \rho(\mathbf{r})\rho_S(\mathbf{r}')u_{sf}(|\mathbf{r} - \mathbf{r}'|) - \mu\int d\mathbf{r}\, \rho(\mathbf{r}) \quad (5)$$

Here $\tilde{F}_{ex}[\rho_S(\mathbf{r}); \rho(\mathbf{r})] = F_{ex}[\rho_S(\mathbf{r}); \rho(\mathbf{r})] - F_{ex}[\rho_S(\mathbf{r}); \rho \equiv 0]$ is the excess Helmholtz free energy of the reference HS fluid, and $F_{ex}[\rho_S(\mathbf{r}); \rho \equiv 0]$ is the excess HS free energy of solid in the absence of fluid.

We employ recent modifications of Rosenfeld's fundamental measure theory[63] for the quenched-annealed mixtures.[60] In the case of hard-core interactions in zero-[60] and one-dimensional limits,[69] it has been shown that the free energy $F_{ex}[\rho_S(\mathbf{r}); \rho(\mathbf{r})]$ for the quenched-annealed mixture has a simple relation to the corresponding free energy of the fully annealed equilibrium HS mixture. Therefore, we assume that FMT functional for equilibrium hard spheres is a good approximation for $F_{ex}[\rho_S(\mathbf{r}); \rho(\mathbf{r})]$. Further improvement of the description of the repulsive term can be achieved by using the modifications,[66,70] which provide a more accurate Carnahan−Starling equation of state in the bulk limit instead of the Percus−Yevick equation.

Unlike for the fluid−fluid interactions, where the WCA scheme gives a reasonably good description of bulk and interfacial properties of simple fluids, the problem of a perturbative treatment of solid−fluid interactions is not straightforward. We present the solid−fluid potential in the form analogous to the WCA scheme:

$$u_{sf}(r) = \begin{cases} 0 & r < r_0 \\ -\epsilon_{sf} & r_0 < r < 2^{1/6}\sigma_{sf} \\ 4\epsilon_{sf}[(\sigma_{sf}/r)^{12} - (\sigma_{sf}/r)^6] & r \geq 2^{1/6}\sigma_{sf} \end{cases} \quad (6)$$

For the reasons discussed below, the potential partition (eq 6) contains a parameter r_0, which limits the range of the constant-energy part of the WCA potential. The standard WCA scheme corresponds to $r_0 = 0$.

(65) Rosenfeld, Y.; Schmidt, M.; Lowen, H.; Tarazona, P. *Phys. Rev. E* **1997**, *55*, 4245−4263.

(66) Yu, Y. X.; Wu, J. Z. *J. Chem. Phys.* **2002**, *117*, 10156−10164.

(67) Figueroa-Gerstenmaier, S.; Blas, F. J.; Avalos, J. B.; Vega, L. F. *J. Chem. Phys.* **2003**, *118*, 830−842.

(68) Sweatman, M. B.; Quirke, N. In *Handbook of Theoretical and Computational Nanotechnology*; Rieth, M., Schommers, W., Eds.; American Scientific Publishers: Stevenson Ranch, CA, 2006.

(69) Reich, H.; Schmidt, M. *J. Stat. Phys.* **2004**, *116*, 1683−1702.

(70) Roth, R.; Evans, R.; Lang, A.; Kahl, G. *J. Phys.: Condens. Matter* **2002**, *14*, 12063−12078.
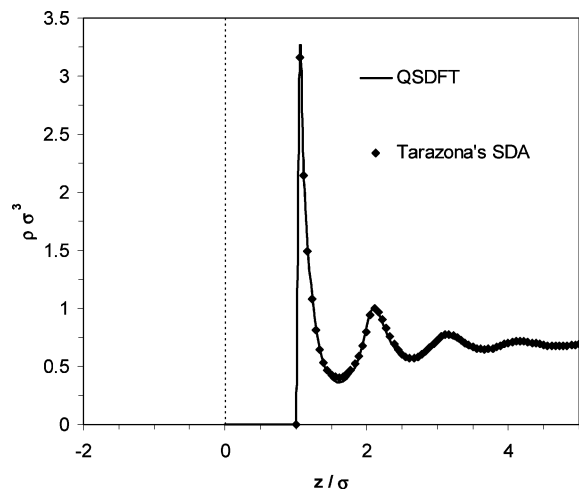
Figure 1. Density profiles for hard-sphere fluid: (—) QSDFT fluid density profile near the solid wall made of hard spheres of effectively infinite density (shown as a vertical dotted line at $z/\sigma = 0$), $\sigma_{ss} = \sigma_{ff}$; (◆) fluid density profile at the hard wall ($z/\sigma = 1$) calculated from Tarazona's SDA.

For a given "quenched" solid density distribution $\rho_S(\mathbf{r})$, the functional (eq 5) is minimized with respect to the fluid density:

$$\left.\frac{\delta\Omega[\rho_S(\mathbf{r});\rho(\mathbf{r})]}{\delta\rho(\mathbf{r})}\right|_{\rho_S(\mathbf{r})} = 0 \qquad (7)$$

that leads to the Euler–Lagrange equation in the form

$$\rho(\mathbf{r}) = \Lambda^{-3}\exp\{c^{(1)}(\mathbf{r};[\rho_S;\rho]) - \beta\int d\mathbf{r}'\,\rho(\mathbf{r})u_{ff}(|\mathbf{r}-\mathbf{r}'|) + \beta\mu - \beta\int d\mathbf{r}'\,\rho_S(\mathbf{r})u_{sf}(|\mathbf{r}-\mathbf{r}'|)\} \quad (8)$$

where $c^{(1)}(\mathbf{r};[\rho_S;\rho]) = -\beta\delta F_{ex}[\rho_S(\mathbf{r});\rho(\mathbf{r})]/\delta\rho(\mathbf{r})$ depends on both the fluid and solid densities.

3. Results and Discussion

First, we consider two limiting cases and compare the QSDFT model with the existing results for the distribution of HS fluid near the hard wall of "infinite" solid density, and adsorption of HS in a HS matrix of constant solid density.

3.1. Hard Spheres near Hard Wall. The QSDFT model reduces to the case of hard wall interactions by setting an infinite density of the solid:

$$\rho_S(z) = \begin{cases} \infty & z < 0 \\ 0 & z > 0 \end{cases} \qquad (9)$$

In this case the excess free energy term of the solid–fluid hard-sphere mixture diverges, which is equivalent to an infinitely large repulsion. In Figure 1 we present a comparison between the density profiles calculated with the Tarazona's SDA[13] and the present approach. In the Tarazona's SDA we set the hard wall potential at $z/\sigma = 1$. The density profiles calculated by two approaches are nearly identical. The fluid is highly structured and exhibits pronounced layering. It should be noted that only when the solid density is numerically very large does the fluid density profile approach the profile for the fluid at the smooth hard wall. This is similar to the case of overlapping hard spheres representing the solid.[61]

3.2. Adsorption of HS in a Hard-Sphere Matrix. Here we consider the case of constant solid density profile. All interactions are hard-core, and QSDFT reduces to the model of annealed HS fluid in quenched HS matrix. In Figure 2, we compare QSDFT adsorption isotherms with GCMC simulations of Kaminsky and
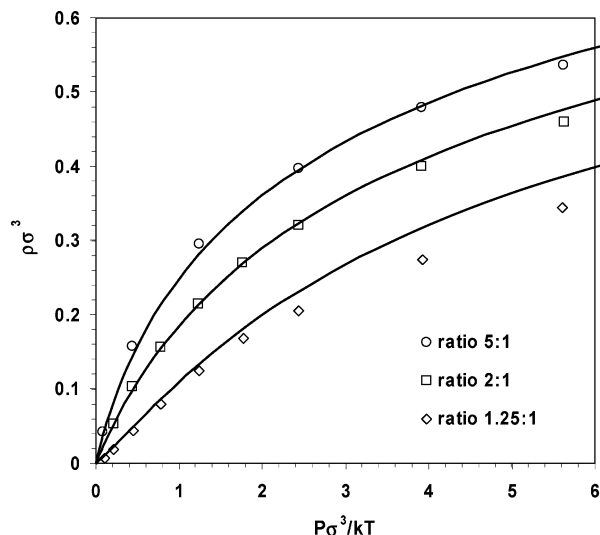

Figure 2. Adsorption of HS in hard-sphere matrix: Comparison of QSDFT (lines) with GCMC simulations[71] (symbols). The packing fraction of the matrix particles is 0.25. The results for three matrix particle:adsorbate particle diameter ratios are shown (1.25:1, 2:1, and 5:1).

Monson[71] for the same system. As expected,[72] the agreement is good, especially for the large size ratio of the solid particles to the fluid particles. Besides validating the numerical calculations, this example demonstrates that QSDFT can effectively account for the microporosity of the solid, which can be described as a penetration of fluid molecules into the solid matrix.

3.3. Fluid in Slit Pores with Attractive Walls. In this section we describe the effect of the solid density distribution on Ar adsorption on a wall with attractive potential. Three different cases are considered: (1) solid wall exerting 9-3 potential (the 9-3 potential is the result of integration of LJ potential with a semi-infinite solid wall located at $z/\sigma_{ff} = 0$), (2) attractive wall with a sharp-kink approximation for the solid density profile, and (3) attractive wall with a diffuse solid density profile. The intermolecular parameters for Ar were taken from ref 19. The parameters of the solid–fluid WCA potential were $\epsilon_{sf}/k_B = 368$ K and $\sigma_{sf} = 0.3$ nm; the density of the solid atoms in the wall was $\rho_0 = 0.07$ Å^{-3}.

The top panel of Figure 3 shows the density profile near the 9-3 wall, calculated by use of the standard FMT model with the modifications that make use of the Carnahan–Starling equation for hard spheres.[66,70] The fluid exhibits strong layering. The middle panel displays QSDFT calculations in which the solid wall has been represented by hard spheres with a sharp-kink density profile. The diameter of solid HS was $d_S = 0.3$ nm, which gives the packing fraction of the solid component close to unity $(\pi/6)\rho_0 d_S^3 = 0.995$. The attractive interactions were included by use of the WCA division of the solid–fluid potential (eq 6), with $r_0 = 0$. The fluid exhibits layering, qualitatively similar to the layering near the 9-3 wall. However, the density peaks are shifted closer to the wall due to the surface roughness, and the tendency for fluid molecules to fill in the cusps between the solid hard spheres. The first fluid peak is located at ca. $0.5\ z/\sigma_{ff}$ from the solid wall. Since the solid packing fraction is very high, it does not permit any penetration of the fluid molecules into the solid matrix.

The bottom panel of Figure 3 presents the density profile near a diffuse, or rough, solid wall with the same solid density in the bulk as in the previous two cases. The solid density distribution

(71) Kaminsky, R. D.; Monson, P. A. *J. Chem. Phys.* **1991**, *95*, 2936–2948.
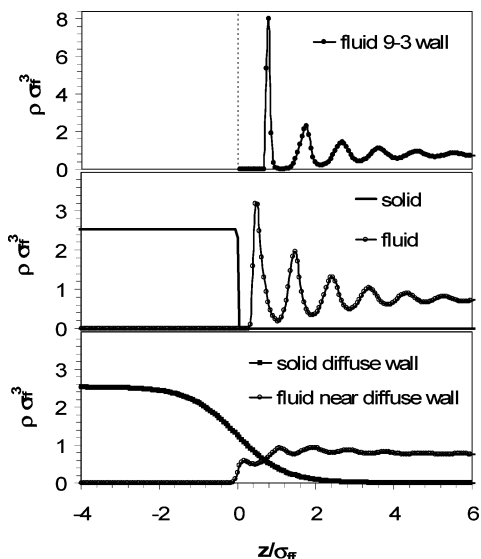(72) Vega, C.; Kaminsky, R. D.; Monson, P. A. *J. Chem. Phys.* **1993**, *99*, 3003–3013.

Figure 3. Density profiles. (a, top panel) LJ fluid density profile at the 9-3 wall calculated by FMT. (b, middle panel) Solid and fluid density profiles calculated by QSDFT and WCA division of the solid−fluid potential. (c, bottom panel) Same as in panel b but with diffuse solid density profile.
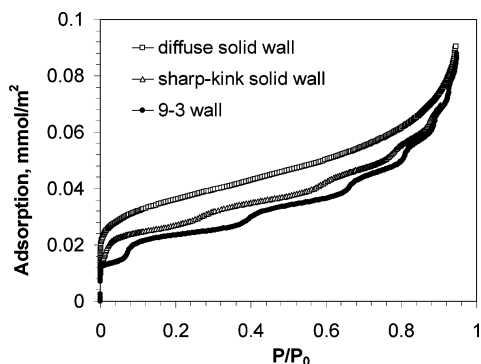

Figure 4. Adsorption isotherms corresponding to the three surface models shown in Figure 3.

is taken in the form that approximates some simulations of amorphous silica surfaces:[34]

$$\rho_S(z) = \frac{\rho_0}{2}\left[1 - \tanh\left(\frac{2(z - z_0)}{\delta}\right)\right] \qquad (10)$$

Here ρ_0 is the solid density in the bulk; $z_0 = 0$ is the position of the solid boundary. The parameter δ characterizes the surface roughness. The solid surface is diffuse ($\delta = 0.8$ nm), which permits additional adsorption on the wall indentations as compared to adsorption on the wall with the sharp, impermeable boundary ($\delta \rightarrow 0$). In the case of the diffuse wall, the fluid density distribution does not exhibit strong layering, although the fluid structure can be clearly seen. Some penetration of the fluid into the solid is also evident.

Figure 4 shows calculated adsorption isotherms. The adsorption isotherms were calculated by integration of the fluid density in the entire simulation box, that is, from H_{min} to H_{max}, which includes the solid boundary z_0:

$$N_S = \int_{H_{min}}^{H_{max}} \rho(z) \, dz \qquad (11)$$

Table 1. Parameters of Intermolecular Interactions for the QSDFT Model of Adsorption on Amorphous Silica Materials

	fluid−fluid[a]		solid−fluid[b]	
	ϵ_{ff}/k_B, K	σ_{ff}, nm	ϵ_{sf}/k_B, K	σ_{sf}, nm
Ar	111.95	0.3358	160.5	0.3104
Kr	155.90	0.3589	189.4	0.322

[a] Diameter of hard spheres, $d_{HS} = \sigma_{ff}$. Fluid−fluid interactions are truncated at $5\sigma_{ff}$. [b] Calculated from the combining rules (see text).

The isotherms are reduced per unit of the smooth wall area, which does not include surface roughness. It can be seen that adsorption per unit area increases with the increase in the extent of surface roughness. The isotherm on a 9-3 wall exhibits pronounced layering steps. The steps become smoother for the sharp-kink solid wall. For the diffuse solid wall, the layering steps are completely absent, and the isotherm is smooth and qualitatively similar to the type II isotherm on amorphous oxides.[24] This example demonstrates that the surface roughness alone can explain the smooth shape of the multilayer adsorption isotherms of typical fluids. It is also remarkable that this result is obtained by use of one-dimensional fluid density distributions.

A comment needs to be made regarding the difference between the isotherms on a 9-3 wall and the sharp-kink solid wall. Even though, the bulk solid density and the interaction parameters are the same, the underlying physical models are different. In the case of a 9-3 wall, the pore wall is perfectly smooth, while the sharp-kink solid wall is inherently rough on the atomic scale. This is why the layering steps are less pronounced. The example in Figures 3 and 4 shows that QSDFT can be used for unified description of adsorption on smooth and rough *atomically structured* surfaces. One way to reproduce the fluid behavior at the *atomically smooth* 9-3 wall as a limiting case of QSDFT is to use some large effective solid density (as in the case of the HS wall) to match the position of the first fluid density peak near the wall. The solid density in the attractive WCA term should be kept, of course, the same as used in the 9-3 potential. The WCA partition itself might need an adjustment, for example, by changing the parameter r_0 in eq 6 in order to match the Henry constant. This possibility will be considered elsewhere.

It is tempting to conclude that one can use the standard NLDFT to describe the fluid behavior near rough walls by using an effective solid−fluid potential with a very soft repulsive tail. Indeed, one can extract such a potential from eq 8 for given solid and fluid density distributions, as it was done in the case of hard-core interactions.[61] However, because $c^{(1)}(\mathbf{r}; [\rho_S; \rho])$ term in eq 8 cannot be split into uncoupled contributions from solid ρ_S and fluid ρ density distributions, the determined effective potential would depend on the chemical potential μ, which makes this approach unfeasible.

3.4. QSDFT Model for Amorphous Silica Surfaces. In the QSDFT model of Ar and Kr adsorption on amorphous silicas, we use the WCA partition for the fluid−solid potential. We use the FMT functional for hard spheres with modifications aimed at correct dimensional crossover for describing narrow cylindrical and spherical pores (RSLT2 version).[65] RSLT2 version uses the Percus−Yevick equation for hard spheres, and, therefore, the parameters of fluid−fluid interactions that describe bulk Ar and Kr differ slightly from the parameters obtained in our previous works[11,73] for the case of Tarazona's NLDFT and the Carnahan−Starling equation for hard spheres. New parameters listed in Table 1 were found from the fit of the bulk coexistence densities and saturation pressure at the normal boiling point of argon and

(73) Neimark, A. V.; Ravikovitch, P. I.; Grun, M.; Schuth, F.; Unger, K. K. *J. Colloid Interface Sci.* **1998**, *207*, 159−169.

krypton. The diameter of hard spheres was kept equal to the LJ fluid–fluid interaction parameter. The potential was truncated at 5 molecular diameters.

Our model for the silica surface is based on the model developed by McElroy and Raghavan (MR);[29] see also ref 30. Fluid–solid interactions are limited to the interactions with oxygen atoms. That is the solid is considered as composed of spheres representing oxygen atoms. The number density of oxygens in the bulk of the material is the same as the density of oxygens in amorphous silica, that is, 0.044 Å^{-3}. The model distinguishes bridging oxygens (BO) in the bulk of the solid and nonbridging oxygens (NBO) near the surface. In the original MR model, the diameter of bridging oxygens was taken as $\sigma_{BO} = 0.27$ nm, and the diameter of nonbridging oxygens was taken as $\sigma_{NBO} = 0.3$ nm, which accounts for the presence of hydrogens. The interaction parameter is the same for both bridging and nonbridging oxygens, $\epsilon_{O-O}/k_B = 230$ K.[30] The parameters of gas–oxygen interactions are calculated from the combining rules (Table 1).

We make the following simplifications. First, we describe the solid using the total oxygen density profile, which includes both bridging and nonbridging oxygens. Second, the diameter of hard spheres representing oxygen ions was taken as $d_O = 0.3$ nm. This value was used as the diameter of nonbridging oxygens in previous simulations of amorphous silica surfaces.[29,30] We found that a smaller value for the oxygen ion diameter (0.27 nm) leads to an unrealistically high degree of penetration of fluid molecules into the solid matrix. We assume that the larger diameter of bridging oxygens effectively accounts for the presence of Si atoms. Third, the distance parameter for the solid–fluid attractive potential was taken as the average of the values for the bridging ($\sigma_{BO} + \sigma_{ff})/2$ and nonbridging ($\sigma_{NBO} + \sigma_{ff})/2$ oxygens. The only remaining parameter of the model is the solid density distribution at the surface. This distribution can be taken, for example, from simulations of amorphous silica surfaces[33,34] or from X-ray diffraction modeling[20,74,75] (see below).

3.5. Argon Adsorption on MCM-41. To demonstrate predictive capabilities of the QSDFT model of amorphous silica, we have chosen an example of Ar adsorption at 87 K on the sample of reference MCM-41 material studied earlier.[6,73] On the basis of the X-ray diffraction data, the total pore volume, and the wall density of 2.2 g/cm^3, the geometrical pore diameter of this material is ~4.5 nm. We modeled the pores as infinitely long cylindrical channels. We performed calculations with two solid density profiles: the function given by eq 10[34] and the linear ramp function that suitably approximates a linearly decreasing oxygen density observed in simulations.[29] Although the exact shape of the solid density profile was found to be of a secondary importance, as compared to the extent of surface roughness, we obtained a somewhat better description of the experimental data by using the linear ramp profile model. In this model, the extent of surface roughness is quantified as the semiwidth of the "ramp". This is the only adjustable parameter in the model.

Figure 5 shows the total oxygen density profile that describes the experimental adsorption data of Ar at 87K on reference MCM-41 material.[73] The geometrical pore size corresponds to $(R - r)/\sigma_{ff} = 0$, that is, the middle of the ramp. The roughness parameter in QSDFT is 0.24 nm. The fluid density distribution is quite smooth, which is in sharp contrast with a layered structure of the fluid at a homogeneous 9-3 wall (Figure 3). Penetration
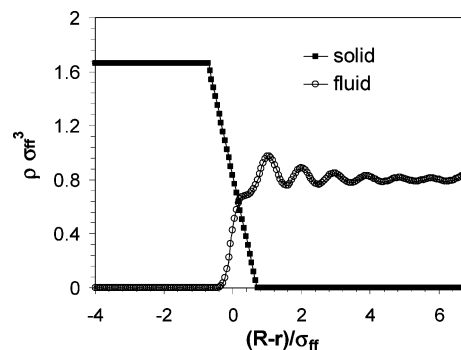
(74) Solovyov, L. A.; Kirik, S. D.; Shmakov, A. N.; Romannikov, V. N. *Microporous Mesoporous Mater.* **2001**, *44*, 17–23.
(75) Hofmann, T.; Wallacher, D.; Huber, P.; Birringer, R.; Knorr, K.; Schreiber, A.; Findenegg, G. H. *Phys. Rev. B* **2005**, *72*.

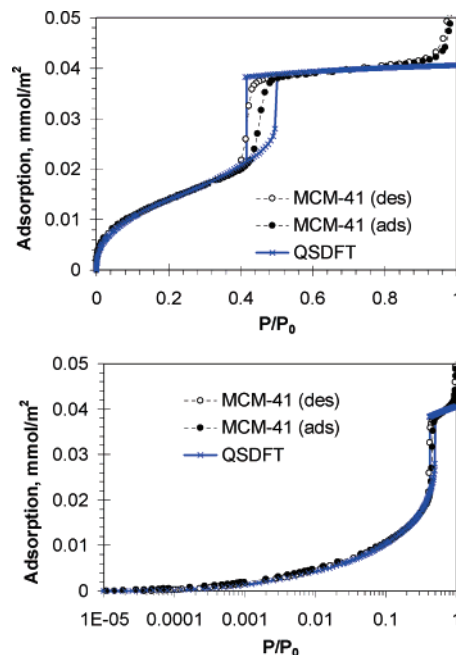**Figure 5.** Density profile of Ar at 87 K in silica cylindrical pore of MCM-41.

Figure 6. Adsorption isotherm of Ar at 87 K in a 4.5 nm diameter MCM-41.

of the fluid into the solid is minimal, which is consistent with the absence of intrawall micropores in MCM-41, and consistent with previous molecular dynamics simulations of adsorption of inert gases on silica surfaces.[31]

Calculated and experimental adsorption isotherms on reference MCM-41 are compared in Figure 6. The agreement is very good in a wide range of relative pressures, starting from $P/P_0 = 1 \times 10^{-5}$. The isotherms are expressed per unit of cylindrical surface area, which does not include molecular roughness. The geometrical surface area of reference MCM-41 is 610 m^2/g—in good agreement with the surface area obtained by NLDFT (620 m^2/g). The experimental isotherm exhibits a narrow hysteresis loop of type H1 according to IUPAC classification. The equilibrium transition pressure corresponds to the experimental desorption branch. The calculated hysteresis loop is wider than the experimental one due to the developing hysteresis effect in pores of 4–5 nm described in ref 7. The width of the hysteresis loop is similar to the results obtained by conventional NLDFT (see Figure 2 from ref 76). This important result demonstrates reliability of both NLDFT and QSDFT for predicting capillary condensation transitions in nanopores.

3.6. Argon Adsorption on Nonporous LiChrosphere Silica. Figure 7 presents the QSDFT calculations of Ar adsorption at

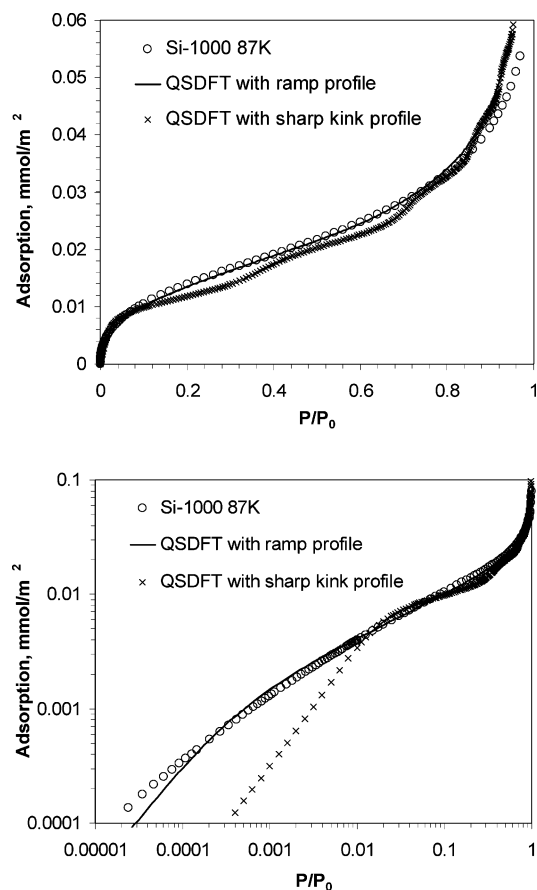(76) Ravikovitch, P. I.; Haller, G. L.; Neimark, A. V. *Adv. Colloid Interface Sci.* **1998**, *77*, 203–226.

Figure 7. Ar adsorption at 87 K on nonporous silica surface. Experimental data on LiChrosphere Si-1000 are from ref 77.

Figure 8. Ar adsorption on nonporous silica surface at 77 and 87 K. Experimental data on LiChrosphere Si-1000 are from refs 77 and 78.

87 K on a nonporous silica surface in comparison with the experimental isotherm on LiChrosphere Si-1000 silica.[77] We performed calculations with a sharp-kink profile, which represents a smooth but atomically structured surface, and with a linear ramp profile characterized by the surface roughness parameter of 0.4 nm. The model with the surface roughness describes the experimental data in a wide range of relative pressures. In contrast, the isotherm for the model with the sharp-kink approximation for the solid density profile exhibits some layering steps, and deviates from the experimental isotherm, especially at the relative pressures below $P/P_0 = 0.01$.

From the comparison of experimental and QSDFT isotherms (Figure 7), the specific surface area of LiChrosphere Si-1000 was found to be 18.3 m^2/g, which does not include surface roughness. It is also of interest to apply the Brunauer−Emmett−Teller (BET) equation to the QSDFT isotherm and to obtain the molecular cross-sectional area of Ar. The BET model applied in the interval of P/P_0 from 0.03 to 0.3 ($R^2 = 0.9995$) gives the cross-sectional area of Ar molecule of 13.4 $Å^2$, and the energetic constant $C = 26.5$. Application of the BET method to the experimental isotherm on Si-1000 in the same interval of relative pressures gives $R^2 = 0.9998$ and $C = 28.6$, which is in excellent agreement with QSDFT. This example demonstrates that QSDFT results are compatible with the classical BET treatment of adsorption isotherms. However, it is worth noticing that QSDFT describes the experimental data practically in the whole range of relative pressures, while the BET model is applicable only in the narrow range of relative pressures.

Figure 8 presents QSDFT calculations on nonporous silica surface for Ar at 77 K in comparison with the experimental data
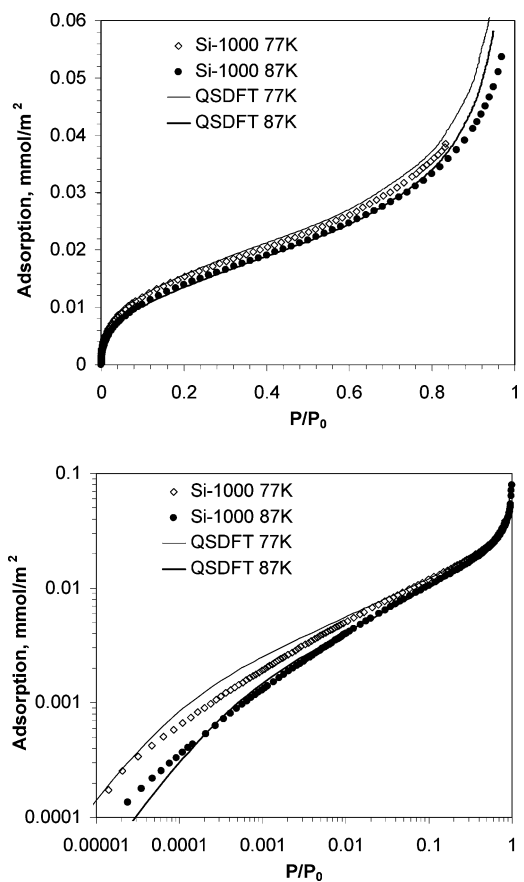
on LiChrosphere Si-1000.[78] Ar at 77 K is below the triple point of the bulk fluid. Following ref 73, the experimental data on LiChrosphere Si-1000[78] were recalculated using the saturation pressure of supercooled liquid Ar (230 Torr). It can be seen that the predictions of QSDFT at 77 K compare quite well with the experimental data, although some deviations at low pressures are apparent. By applying the BET method to the QSDFT isotherm in the range of relative pressures P/P_0 from 0.03 to 0.3 ($R^2 = 0.9996$), we obtained the cross-sectional area of Ar at 77 K as 11.9 $Å^2$ and the constant $C = 34$. By applying the BET method to the experimental isotherm at 77 K we obtained $C = 36$ and $R^2 = 0.9998$—again, in very good agreement with QSDFT.

It should be noted that even though no optimization was performed in order to find the best solid density distribution or parameters for solid−fluid interactions, the success of QSDFT in predicting adsorption isotherms on amorphous silica surface at two different temperatures is quite remarkable.

3.7. Krypton Adsorption on SBA-15 Silica. In this section we test the QSDFT model by predicting adsorption of Kr on SBA-15 using information on the surface roughness obtained from modeling X-ray diffraction.[75] Parameters for Kr−Kr interactions were fitted to the bulk properties of Kr. We used the same model for the silica surface as was used for predicting Ar adsorption on MCM-41 and Si-1000 (except for the extent of the surface roughness). The Kr−oxygen interaction parameters were obtained from the combining rules (Table 1).

Hofmann et al.[75] studied Kr adsorption in SBA-15 at 119 K. They used the "corona" model of SBA-15 to analyze small-angle X-ray diffraction patterns and to calculate the radial position

(77) Kruk, M.; Jaroniec, M. *Chem. Mater.* **2000**, *12*, 222−230.

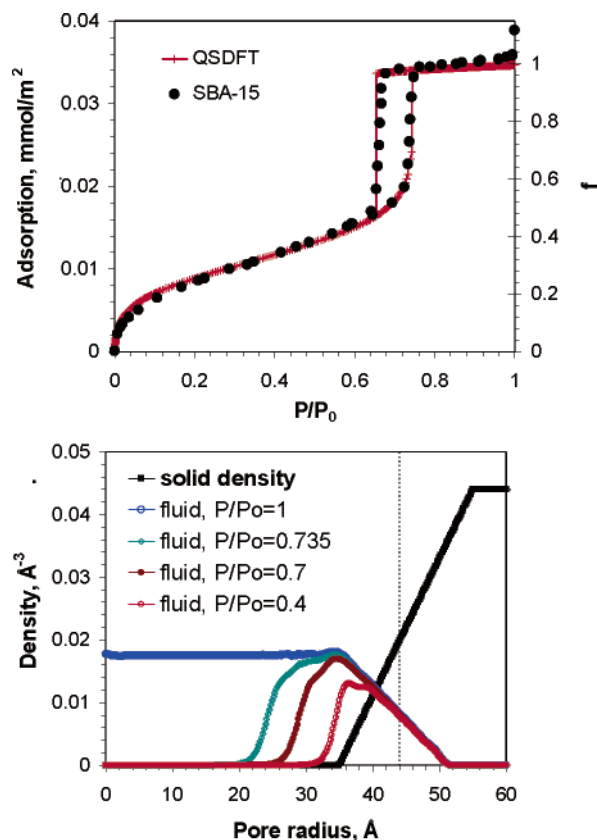(78) Kruk, M.; Jaroniec, M. *J. Phys. Chem. B* **2002**, *106*, 4732−4739.

Figure 9. (Top) Prediction of krypton adsorption on SBA-15 silica at 119 K. Experimental data are from ref 75. (Bottom) Density profiles of solid (squares) and fluid at different pressures along the adsorption branch. Thin vertical line at $r = 43.9$Å indicates the pore radius at which the excess fluid density is zero. The solid excess mass is zero at $r = 45$ Å.

of the liquid–vapor interface and film roughness. Their model is similar to the model used by Imperor-Clerc et al.,[20] who described the corona density using a linear ramp function.

In the QSDFT calculations we used the solid density profile obtained from X-ray diffraction modeling[75] (Figure 9, bottom panel). The roughness parameter was set to 1 nm, which corresponds to the value reported in ref 75. Excellent agreement with the experimental isotherm was found for the pore diameter of 9 nm (Figure 9). It is worth noticing that although this value is slightly larger than the value of 8.4 nm reported in ref 75, the pore diameter determined from the condition of zero excess fluid density is 8.8 nm. QSDFT predicts quantitatively the smooth multilayer adsorption isotherm on a rough surface and the entire hysteresis loop, including adsorption and desorption branches. The equilibrium transition corresponds to the experimental desorption branch. This example corroborates the picture of the pore wall surface of SBA-15 materials as being very rough (~1 nm) because consistent results have been obtained from X-ray diffraction[75] and adsorption by using the same model for SBA-15 surface. Note a high degree of penetration of Kr into SBA-15 matrix (Figure 9, bottom panel), which is in contrast with dense amorphous silica and glass surfaces.[31]

3.8. Solvation Pressure in Amorphous Silica Nanopores. In another paper[79] we show that, for materials with narrow pore size distributions, the solvation pressure exerted by the fluid on the pore walls is linked to the skeleton deformation (swelling or shrinking) in the course of adsorption. For Kr and Ar in zeolites X, experimentally observed changes of the adsorbent volume
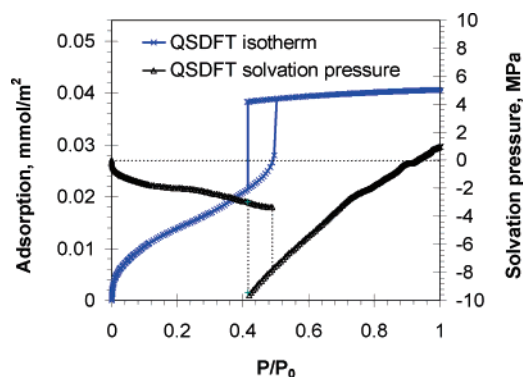
(79) Ravikovitch, P. I.; Neimark, A. V. *Langmuir* **2006**, *22*, 10864–10868.

Figure 10. Adsorption isotherm of Ar at 87 K in a 4.5 nm cylindrical pore and calculated solvation pressure.

(strain) were shown to be proportional to the solvation pressure.[79] In the following example, we employ QSDFT to calculate solvation pressure isotherm in a cylindrical mesopore of MCM-41 material. Following ref 79, we calculate the solvation pressure in a cylindrical pore of radius R as

$$\sigma = -\frac{1}{2\pi RL}\left(\frac{\partial \Omega}{\partial R}\right)\bigg|_{\mu,T} - p_{bulk} \tag{12}$$

where R is the pore radius, L is the pore length, Ω is the grand potential calculated from eq 5, and p_{bulk} is the bulk pressure.

Figure 10 presents the results of calculations for the pore 4.5 nm in diameter. The solvation pressure is negative and gradually decreases in the process of multilayer adsorption. At the capillary condensation transition, the solvation pressure sharply decreases to the minimum value and then gradually increases and changes sign at P/P_0 close to the bulk saturation pressure. The calculated hysteresis loop of the solvation pressure isotherm is qualitatively similar to the hysteresis loops reported experimentally for the strain isotherms in porous materials[80] and thin porous films.[81–83] This example demonstrates the potential of using QSDFT for interpretation of adsorption deformation measurements and characterization of mechanical properties of porous materials.

Conclusions

We have presented a novel quenched solid density functional theory (QSDFT) model of adsorption on amorphous and microporous silicas, in which solid atoms are considered as quenched component(s) of the solid–fluid mixture with a fixed density distribution. Repulsive interactions were described with the multicomponent FMT functional for hard spheres. Attractive interactions were treated with the WCA scheme. There are several advantages of considering the solid as a quenched component of the fluid–solid system rather than the source of an external potential field. On one hand, this approach offers flexibility in the description of the fluid–solid boundary by varying the solid density and the thickness of the diffuse solid surface layer. On the other hand, it retains the main advantage of NLDFT—its computational efficiency, because even a one-dimensional solid density distribution can account for the effects of surface roughness and heterogeneity.

QSDFT provides a unified model of adsorption on both smooth (Figures 3b and 7) and rough (Figures 3c and 7) atomically

(80) Haines, R. S.; McIntosh, R. *J. Chem. Phys.* **1947**, *15*, 28–38.
(81) Dolino, G.; Bellet, D.; Faivre, C. *Phys. Rev. B* **1996**, *54*, 17919–17929.
(82) Mogilnikov, K. P.; Baklanov, M. R. *Electrochem. Solid State Lett.* **2002**, *5*, F29–F31.
(83) Boissiere, C.; Grosso, D.; Lepoutre, S.; Nicole, L.; Bruneau, A. B.; Sanchez, C. *Langmuir* **2005**, *21*, 12362–12371.

structured surfaces. QSDFT describes the behavior of LJ fluid near a smooth hard wall by employing a uniform solid density distribution with a packing density approaching infinity (Figure 1). The behavior of LJ fluid near a smooth attractive wall can be achieved by using an appropriate division of the solid−fluid potential into repulsive and attractive parts (eq 6). As a limiting case of uniform solid density, QSDFT also provides good description of adsorption in random solid matrices, which can be considered as micropores.

The main strength of the proposed model is the description of the surface roughness. The solid density distribution can be taken from simulations of amorphous silica surfaces[33,34] or directly from experiments.[75] We have demonstrated that by using an established molecular model of silica structure,[29] and using a total distribution of bridging and nonbridging oxygens as an input, QSDFT provides quantitative predictions of adsorption isotherms on MCM-41, amorphous LiChrosphere silica, and SBA-15 silica materials with a minimal number of adjustable parameters. The results for the surface roughness of SBA-15 obtained from QSDFT are in very good agreement with X-ray diffraction modeling, with both approaches predicting ca. 2 nm thick layer of gradually decreasing density silica. We are currently studying transferability of the model to different temperatures and pore sizes. Possible extensions of the model can include more detailed accounting for the surface active sites as well as organic modifications of silica surfaces that can be introduced as third and fourth components, etc.

We have also calculated the solvation pressure isotherms in silica nanopores of MCM-41 and found that they are in qualitative agreement with the adsorption deformation measurements in mesoporous materials. We conclude that QSDFT is a very promising tool that can be used for characterization of silica materials, including micro−mesopore size distribution, adsorption deformation, and surface roughness/heterogeneity.